https://doi.org/10.1016/j.corsci.2017.06.001

Synthesis of well-aligned CuO nanowire array integrated with nanoporous CuO network for oxidative degradation of methylene blue

R. Li[1,2], K. C. Chan[1]*, X. J. Liu[2], X. H. Zhang[3], L. Liu[4], T. Li[5], Z. P. Lu[2]*

1. Advanced Manufacturing Technology Research Centre, Department of Industrial and Systems Engineering, The Hong Kong Polytechnic University, Hong Kong

2. State Key Laboratory for Advanced Metals and Materials, University of Science and Technology Beijing, Beijing 100083, P. R. China

3. Jiangsu Key Laboratory of Advanced Metallic Materials, School of Materials Science and Engineering, Southeast University, Nanjing 211189, China

4. School of Materials Science and Engineering, Huazhong University of Science and Technology, Wuhan 430074, China

5. School of Chemistry and Chemical Engineering, Huazhong University of Science and Technology, Wuhan 430074, China

Abstract

In this paper, we report the fabrication of a 3D free-standing CuO nanowire array supported by nanoporous CuO network by dealloying $Cu_{60}Zr_{35}Al_5$ glassy ribbon and the subsequent thermal oxidation. The CuO nanocomposite exhibits a hierarchical nanostructure containing well-aligned CuO nanowire arrays and nanoporous substrate with continuous nanoporosity. The resulting nanocomposite product with high internal surface area shows superior degradation performance for methylene blue in the presence of H_2O_2 than that of commercial CuO nanoparticles. The remarkable catalytic

*Corresponding author. E-mail: kc.chan@polyu.edu.hk or luzp@ustb.edu.cn

activity along with good reusability and stability during degradation make the as-prepared nanocomposite a promising candidate for purifying wastewater with organic dyes.

Keywords: A. Copper; A. Glass; C. Acid corrosion; C. Oxidation.

1. Introduction

In recent years, as important organic chemical raw materials, dyes are widely used in the textile, paper and plastics industries, however, due to the high content of organic compounds and high environmental stability of synthetic dyestuffs, their unrestricted discharge into water greatly endangers the environment [1-3]. Consequently, degradation of organic contaminants in industrial wastewaters has become a research focus and is receiving increasing attention. Over the past decades, in the treatment of dye polluting water, traditional approaches such as ultra-filtration, flocculation and adsorption onto active carbon have raised difficulties in the complete destruction of organic contaminants and also have further negative factors in potentially secondary contamination due to the high chemical stability of these organic contaminants [4-7]. Recently, oxidation methods have been considered as a sustainable technique to remove environmental pollutants from wastewater, in which highly reactive hydroxyl radicals (·OH) are produced and give rise to the oxidative degradation process of the synthetic dyes [8-10]. In this method, many metal oxide nanoparticles, including TiO_2, Fe_3O_4, SnO_2 and CuO, have been produced to provide oxidative degradation of various organic dyes such as methylene blue (MB), methylene orange (MO) and Rhodamine 6G (R6G) in wastewater [11-15]. Among them, oxidative degradation of organic dyes by CuO based nanoparticles has received considerable attention due to its low cost, high efficiency and environmental stability. However, the powdery CuO nanoparticles easily aggregate during oxidation due to their high surface energy, which significantly decreases the catalytic efficiency and lifetime. In addition, the complex reclamation

process of CuO nanoparticles from the treated water is also a disadvantage to their practical industrial application [16, 17]. Therefore, the development of high-performance nanostructured CuO based catalysts is still a challenge.

It is known that the degradation performance of the nanocatalysts often depend on their effective surface area and porosity [18]. It is of great importance to tailor the morphology, distribution and nanostructure of the catalysts during synthesis and more and more research has been carried out to investigate the synthetic pathways of various hierarchical nanostructures [19, 20]. For CuO based nanocatalysts, the properties are also closely related to the microstructure, particularly the orientation and surface morphology [21]. To date, besides nanoparticles, CuO nanostructures with diversified controlled shapes, including nanospheres, nanoplates, nanorods and nanowires also have been synthesized by aqueous solution decomposition, hydrothermal method, and thermal oxidation [22-24]. Though various synthetic methods are reported for the fabrication of nanostructured CuO, it is still highly desirable to develop novel and smart synthetic procedures for building the hierarchical CuO micro/nanostructure with outstanding catalytic performance. Recently, three dimensional (3D) nanoporous metals/metal oxides with uniform nanopore structure and well-controlled size have been extensively applied in catalysts due to their large internal surface area and open nanoporosity [25-27]. By using nanoporous metal/metal oxides as a template, it is possible to prepare nanocatalysts with a hierarchical nanostructure, high surface area and large pore volume. Herein, for the first time, we demonstrate the synthesis of a 3D hierarchical CuO nanowire array modified nanoporous CuO nanocomposite with a

well-aligned nanowire distribution and high internal surface area by oxidative thermal treatment of the monolithic nanoporous Cu substrate. In this study, the catalytic capability of the as-synthesized CuO nanocomposite was systematically investigated for the oxidative degradation of MB in the presence of hydrogen peroxide (H_2O_2). The hierarchical nanostructure exhibits remarkable degradation activity for organic dyes with good cycling stability, demonstrating great potential for purifying wastewater.

2. Experimental

2.1. Preparation of nanoporous Cu as substrate.

A nanoporous Cu substrate was fabricated by chemical dealloying of $Cu_{60}Zr_{35}Al_5$ metallic glass, as described in our previous paper [28]. Briefly, the typical $Cu_{60}Zr_{35}Al_5$ (nominal atomic percentage) glassy ribbon precursor with a width of 4 mm and a thickness of ~25 μm was prepared by a melt-spinning technique under a high purity argon atmosphere. The nanoporous Cu ribbon was then produced by leaching the $Cu_{60}Zr_{35}Al_5$ glassy ribbons in a dilute HF aqueous solution with a concentration of 0.05 mol/L at room temperature for 12 h. The dealloyed products were repeatedly rinsed with deionized water and dehydrated alcohol to remove residual chemicals within the pore channels.

2.2. Synthesis of CuO nanowire array modified nanoporous CuO nanocomposite.

Synthesis of CuO nanowire array was carried out by thermal oxidation of the nanoporous Cu ribbon: the cleaned nanoporous Cu substrate was placed in a corundum crucible and then heated to 500 °C in air. The samples were held at the chosen

temperature for 4 h and the heating rate was fixed at 10 °C/min. A vertically aligned CuO nanowire array modified nanoporous CuO nanocomposite was then obtained. After cooling to room temperature, the as-prepared nanocomposites were repeatedly rinsed with deionized water and dehydrated alcohol.

2.3. Microstructure characterization.

X-ray diffraction (XRD, Rigaku DMAX-RB-12KW, Cu-Kα) was used to determine the crystal structures of the samples. The microstructures of the nanostructured materials were characterized by scanning electron microscopy (SEM, Zeiss Supra 55) equipped with an energy dispersive X-ray spectrometer (EDX) and transmission electron microscope (TEM, Tecnai G2 F30). For TEM studies, the as prepared samples were dispersed by sonication in absolute ethyl alcohol and the resultant suspensions were put onto holey carbon-supported copper grids. X-ray photoelectron spectroscopy (XPS AXIS-ULTRA-DLD, Kratos) with an Al Kα (mono, 1486.6 eV) anode at an energy of 150 W in a vacuum of 10^{-7} Pa was also employed to investigate the surface chemical state and binding energy of the samples. Before each XPS measurement, the selected samples were rinsed in dehydrated alcohol to remove residual chemicals and then sealed in an argon atmosphere to avoid possible oxidation. A Brunauer-Emmett-Teller (BET) test was carried out to measure the internal surface area of the sample by using an automated surface area and pore size analyzer (Quadrasorb SI).

2.4. Evolution of methylene blue degradation performance.

The catalytic performance of the nanocomposite was investigated by measuring

the decomposition rate of MB, with or without the presence of H_2O_2, in a neutral condition. All degradation tests were carried out in 250 mL bottles with a thermostatic water bath. The catalyst sample was added into the MB solution, followed by the addition of the H_2O_2 solution. During each degradation, the mixed MB solutions were rod-stirred at a constant speed. After the reaction, 3 mL of filtered solution was pipetted out and subjected to UV-vis spectrum scanning ranging from 200 to 800 nm using a UV spectrophotometer (UV-2800, Unico). Before testing, a decreased concentration was used to meet the maximum intensity of the UV measurement. The degradation activities of the nanocomposite with MB dye were then systemically investigated with different reaction conditions, including H_2O_2 concentrations, sample dosages, MB concentrations and reaction temperatures.

3. Results and Discussion

3.1. Synthesis and characterization of the CuO nanowire array modified nanoporous CuO nanocomposite.

A two-step procedure was performed to fabricate the 3D hierarchical CuO nanowire array modified nanoporous CuO nanocomposite. The first step is the fabrication of the nanoporous Cu substrate by the dealloying method. It is known that metallic glasses which possess a homogeneous structure and are free from crystallographic defects have apparent advantages for utilization as precursors for fabricating homogeneous nanoporous metals **[29, 30]**. In the case of crystalline precursors, they have a narrow composition range to form single-phase microstructure and the unavoidable crystalline defects, such as grain boundary, dislocation or

segregation, are also disadvantageous to the formation of uniform nanoporosity **[31, 32]**. Thus, in order to obtain a uniform nanoporous Cu substrate, a classical $Cu_{60}Zr_{35}Al_5$ amorphous metallic glass precursor was selected. In this alloy, Cu is much more noble than Zr and Al, i.e., the standard equilibrium electrode potentials for the Cu/Cu^{2+}, Zr/Zr^{4+} and Al/Al^{3+} pairs are +0.337 V_{SHE}, -1.553 V_{SHE} and -1.65 V_{SHE}, respectively, which offer an advantageous driving force for the dissolution of less noble elements Zr and Al under free corrosion condition. Similar to the corrosion behavior during the chemical dealloying of Pd-Ni-P, Ag-Mg-Ca and Mg-Cu-Y metallic glasses **[29, 33, 34]**, due to the combined action of the dissolution process of the Zr and Al atoms and the surface diffusion of the Cu atoms at the glassy precursor/solution interface, nanoporous Cu ribbon with a uniform bi-continuous nanoporosity was fabricated by etching the $Cu_{60}Zr_{35}Al_5$ glassy ribbon in 0.05 mol/L HF aqueous solution for 12 h at room temperature. The thermal oxidation treatment of the dealloyed nanoporous Cu ribbon was then carried out at the chosen temperature of 500 °C in air for 4 h to produce the CuO nanowire array modified nanoporous CuO nanocomposite. **Fig. 1** shows the XRD patterns of the $Cu_{60}Zr_{35}Al_5$ glassy ribbon, dealloyed nanoporous Cu and heated nanostructured CuO, respectively. It is seen that the characteristic amorphous halo of the $Cu_{60}Zr_{35}Al_5$ glassy precursor completely disappears after dealloying and sharp crystalline peaks representative of the pure face-centered (*fcc*) Cu emerge. Due to the heat treatment, the characteristic crystalline peaks of monoclinic CuO appear and other oxidation states of Cu are invisible, demonstrating a high purity of the generated nanostructured CuO.

Figs 2a and **b** show the cross-sectional and surface morphologies of the dealloyed nanoporous Cu ribbon, respectively, which exhibits a uniform nanoporosity throughout the sample with connected pore channels and ligaments. EDX analysis of the cross section (the inset in **Fig. 2a**) demonstrates that the Zr and Al elements were completely leached out from the glassy precursor, and the residual metals with nanopores were pure Cu. SEM image of the nanoporous Cu ribbon after it had been heated in air at 500 °C for 4 h is presented in **Fig. 2c**, where the entire surface of the substrate is covered by a high density of CuO nanowires with similar quality and good uniformity. The cross-sectional view of the oxidized sample in the inset of **Fig. 2c** displays an obvious interface of the nanowire arrays and the growing template, and it is also found that the porous structure of the nanoporous Cu has been retained during oxidation, forming a hierarchical structure which contains a nanoporous CuO region in-between and CuO nanowire array layers on the surfaces. **Fig. 2d** further shows the surface morphologies of the as-prepared CuO nanocomposite, it is seen that after the thermal oxidative treatment, the CuO nanowires grew uniformly on the surface of the nanoporous substrate. It is known that CuO nanowires are generally formed at grain boundaries, flaws or defects due to the rapid, short-circuit diffusion of the Cu ions **[35, 36]**. Based on this, we discuss the growth mechanism of the CuO nanowire array structure. Initially, a CuO layer is formed during the heating treatment and due to the porous structure of the nanoporous Cu substrate, such a CuO layer is highly porous and defective (inset in **Fig. 2c**). Then, CuO nanowires are generated as a result of the short-circuit diffusion of the Cu ions across the pores and gaps of the nanoporous CuO substrate. Meanwhile,

owing to the uniform distribution of the nanoporosity of the substrate, the arrangement of the CuO nanowires naturally tends to be homogeneous. Eventually, the uniform CuO nanowire array structure emerges.

We further characterize the structure and crystallinity of the typical nanowires using TEM and electron diffraction. The low-magnification TEM image (**Fig. 3a**) of a single CuO nanowire shows that the width of the nanowire is about 120 nm and the length is over 1 μm. **Fig. 3b** shows the corresponding SAED pattern of the CuO nanowire. The electron beam is along the [001] zone axis and the diffraction spots can be indexed as the (-110), (110) and (020) reflections of the CuO. From the HRETM image (**Fig. 3c**), the interplanar spacing of the CuO nanowire is measured to be ~0.27 nm, which agrees well with the (110) lattice fringe of the monoclinic CuO. These results both confirm that the as-grown nanowire is indeed single-crystalline CuO.

The chemical composition and purity of the hierarchical CuO nanocomposite were further investigated by XPS. As shown in **Fig. 4a**, the high-resolution XPS spectrum for the Cu 2p core level shows two peaks at 934.2 eV and 954.2 eV, corresponding to a spin-orbit couple of Cu $2p_{3/2}$ and Cu $2p_{1/2}$ respectively, indicating the presence of the Cu^{2+}. Extra satellite peaks at 941.6 eV and 944.2 eV for Cu $2p_{3/2}$ and 962.5 eV for Cu $2p_{1/2}$ were also observed at the higher binding energy side, which implies the presence of a characteristic d^9 Cu(Ⅱ) compound **[35]**. The whole XPS spectrum in the study also indicates that the as-prepared nanocomposite is composed of copper, oxygen and trace carbon, confirming the high purity of this product (not shown). Furthermore, the N_2 adsorption-desorption isotherms of the as-prepared CuO nanocomposite was used

to determine the BET specific surface area (**Fig. 4b**), and remarkably, the product exhibits an average BET specific surface area of 27.16 m^2/g, much higher than that of the dealloyed nanoporous Cu (15.96 m^2/g), demonstrating that after the thermal oxidative treatment, the surface area of the CuO nanocomposite increases due to the generation of the CuO nanowire array structure. The pore size distribution of the nanocomposite is illustrated in the **Fig. 4b** inset, and the curves show the relative pore volume distributions according to the average of pore size, in which the size of the pores is in the range of 10 to 90 nm. The high surface area of the CuO nanocomposite may originate from the small nanoparticle size of the as-grown CuO nanowires and the retained nanoporous structure of the substrate.

3.2. Oxidative degradation capability of methylene blue.

To explore the potential capability of the CuO nanocomposite product to degrade organic contaminants from wastewater, the catalytic activity of the hierarchical CuO nanostructures is evaluated in the oxidation of MB in the presence of H_2O_2 under neutral condition. **Fig. 5a** shows the UV adsorption spectra of 0.1 g/L MB aqueous solution in the presence of a 2 g/L CuO nanocomposite and 0.5 mol/L H_2O_2 for different reaction times at room temperature. Clearly, the characteristic absorption peak of the MB is located around 665 nm and with the prolonged treatment time, the adsorption peak of the MB drops. After 70 min, the band at 665 nm becomes very broad and weak, and no obvious peak shift can be observed, suggesting the continuous degradation of MB dye. The appearance of the MB solution is also shown in the inset of **Fig. 5a**. As can be seen, before the treatment, the solution has a dark blue color. Finally, the dye can be almost

completely degraded by the CuO nanocomposite and the solution becomes almost transparent. This indicates that the CuO nanocomposite has good reaction activity and can thoroughly decompose MB dye. For comparison, contrast experiments are carried out, in which the bare $Cu_{60}Zr_{35}Al_5$ glassy ribbon, dealloyed nanoporous Cu and commercial CuO nanoparticles (particle size: 50-200 nm, specific surface area: > $18m^2/g$) are used as catalysts while other conditions are kept unchanged. By measuring the intensity of the MB adsorption peak at 665 nm, the concentration variation of DB against reaction time for different catalysts are obtained and presented in **Fig. 5b**. It is seen that the normalized concentration (c/c_0) of MB has changed little in the absence of the catalyst, suggesting that H_2O_2 alone can hardly oxide MB in this case. When the bare $Cu_{60}Zr_{35}Al_5$ glassy ribbon or nanoporous Cu is used as catalyst, the degradation is still very slow, suggesting that these materials have weak catalytic capability in the oxidative degradation of MB with H_2O_2 in the study. It is also found that c/c_0 of MB drops to 0.307 after 70 min for the commercial CuO nanoparticles. The c/c_0 of MB is only 0.03 at the reaction time of 70 min when the as-synthesized hierarchical nanostructured CuO is presented, indicating that our CuO nanocomposite product has a higher degradation performance than that of commercial CuO nanoparticles. The reasons for the superior catalytic ability of the as-prepared CuO nanocomposite is discussed. For the particulate CuO nanocatalyst, agglomeration during the decomposition process significantly decreases the active surface of the catalyst and thus reduces the degradation ability. In our case, in contrast to the CuO nanoparticles, the monolithic CuO nanocomposite with equally distributed CuO nanowire arrays can

avoid particle agglomeration and possesses more active sites for the catalytic reaction, resulting in an enhanced degradation performance. Moreover, the high internal surface area contributed from the open pore structure of the nanoporous substrate also provides more effective contact between the MB and catalyst, leading to the significant improvement of the oxidative degradation performance of the CuO nanowire array modified nanoporous CuO product.

It is widely known that degradation conditions have a great influence on the degradation efficiency of heterogeneous catalysis **[38, 39]**. In our work, different amounts of H_2O_2 concentration, catalyst dosage, initial MB concentration and reaction temperature, are used to investigate their effects on the oxidative degradation performance of MB by the CuO nanowire array modified nanoporous CuO nanocomposite. The effect of initial H_2O_2 concentration ranging from 0 to 0.6 mol/L on the degradation of 0.1 g/L MB solution by 2 g/L CuO nanocomposite is presented in **Fig. 6a**. It is seen that the degradation rate of MB increases with the increase of H_2O_2 concentration from 0 to 0.5 mol/L and then decreases when the concentration is further increased. This may be because, a high H_2O_2 concentration is favorable for the formation of the highly reactive ·OH and preferentially attacks the MB molecules, inducing a higher degradation rate. However, an excessive H_2O_2 concentration will act as a scavenger of the ·OH **[40, 41]**, which may result in the reduction of the radical activity and bring a detrimental impact on the MB degradation. **Fig. 6b** shows the effect of the CuO nanocomposite dosage on the degradation efficiency of 0.1 g/L MB solution in presence of 0.5 mol/L H_2O_2, At the same reaction time, with increasing the CuO

nanocomposite dosage from 0.5 to 10 g/L, the c/c_0 of the MB significantly decreases, suggesting that the degradation efficiency of MB is enhanced with increase in the CuO nanocomposite dosage. Considering the low cost of CuO, it is economical to use a high dosage of CuO nanocomposites to improve the degradation rate. The effect of different initial MB concentrations ranging from 0.1 to 0.3 g/L on the degradation efficiency was also investigated (**Fig. 6c**). It is shown that the degradation time increases as the initial MB concentration increases. Moreover, investigations on the influence of atmosphere temperature were performed to evaluate the activation energy for the oxidative degradation of MB with the CuO nanocomposite. As shown in **Fig. 6d**, the degradation accelerates significantly as the increase of reaction temperature increases from 25 to 55 °C. Based on the reaction rate constants at different temperatures, obtained by data fitting, the activation energy can be then calculated according to the following Arrhenius-type equation **[38, 42]**:

$$\ln k_T = {E_a}/{RT} + \ln A$$

where T is the reaction temperature, k_T is the kinetic rate constant, E_a is the activation energy, R is the gas constant and A is a constant. The plot of $\ln k_T$ versus $1000/\mathrm{RT}$ is presented in the inset of **Fig. 6d**. Clearly, a good linear relationship is obtained and the calculated activation energy is approximately 38.5 kJ/mol. The value is low when compared with the oxidative degradation process by ferrocene catalysts through Fenton-like reaction in the presence of H_2O_2 **[43]**.

To further confirm the degradation ability of the CuO nanowire array modified nanoporous CuO, we also investigated the reusability and stability of the nanocatalyst.

In this study, without any centrifugalization or filtration, the monolithic hierarchical CuO nanocatalyst can be easily separated from the reacted wastewater. After cleaning using deionized water, the recovered sample can be reused again. **Fig. 7a** illustrates the decomposition ratio of MB at 70 min for different cycles, where it is seen that the degradation ratio still remains ~88.5% after 5 cycles, showing that there is no obvious loss of the degradation activity for our nanostructured product during cycling. **Fig. 7b** also presents the surface morphology of the recovered CuO nanocatalyst after 5 catalytic cycles, where the SEM image reveals that in comparison with the initial composite (**Fig. 2d**), there is no significant change in the microstructure of the nanostructured CuO during multiple cycles. EDX analysis in the inset of **Fig. 7b** also shows that the composition of the sample is still CuO after several decolorization treatments. These results demonstrate that our CuO nanowire array modified nanoporous CuO catalyst has good reusability and stability for oxidative degradation of MB. The long-term stability and good reusability of the CuO nanocatalyst during degradation can be attributed to the chemical durability of CuO and the structural stability of the CuO nanowire arrays.

4. Conclusions

In summary, a uniform CuO nanowire array integrated with nanoporous CuO nanocomposite was prepared by the combination of chemical dealloying of $Cu_{60}Zr_{35}Al_5$ glassy ribbon with thermal oxidation of dealloyed nanoporous Cu. The CuO nanocomposite presents a hierarchical nanostructure with a uniform nanowire array and

3D open pore nanoporosity, the surface area of which is measured to be ~27.16 m^2/g. The as-synthesized monolithic hierarchical CuO nanocomposite exhibits superior oxidative degradation performance for MB in the presence of H_2O_2 than that of commercial CuO nanoparticles. It is found that the high degradation efficiency of the nanocomposite mainly results from the uniform nanowire array structure and its high internal surface area, which can provide more effective contact between the MB and catalysts. The present study also indicates that the CuO nanocomposite possesses good reusability and long-term stability, which results from the chemical durability and the structural stability of the CuO nanocatalyst.

Acknowledgements

This research was supported by the Research Grants Council of the Hong Kong Special Administrative Region, China (Project No. PolyU 511313). This research was also supported by International S&T Cooperation Program of China (2015DFG52600) and program for Changjiang Scholars and Innovative Research Team in University of China(IRT_14R05).

References

[1] H. R. Guendy, Enhancing of textile wastewater treatment using different catalysts for advanced oxidation process, Aust. J. Basic Appl. Sci. 3 (2009) 4046-4052.

[2] W. X. Zhang, Nanoscale iron particles for environmental remediation: an overview, J. Nanoparticle Res. 5 (2003) 323-332.

[3] V. K. Gupta, Suhas, Application of low-cost adsorbents for dye removal-A review, J. Environ. Manage. 90 (2009) 2313-2342.

[4] Y. Chen, K. Wang, L. P. Lou, Photodegradation of dye pollutants on silica gel supported TiO_2 particles under visible light irradiation, J. Photochem. Photobiol. A 163 (2004) 281-287.

[5] A. N. Ejhieh, H. Z. Mobarakeh, Heterogeneous photodecolorization of mixture of methylene blue and bromophenol blue using CuO-nano-clinoptilolite, J. Ind. Eng. Chem. 20 (2014) 1421-1431.

[6] B. H. Hameed, A. L. Ahmad, K. N. A. Latiff, Adsorption of basic dye (methylene blue) onto activated carbon prepared from rattan sawdust, Dyes Pigments 75 (2007) 143-149.

[7] S. Meriça, H. Selçukb, V. Belgiorno, Acute toxicity removal in textile finishing wastewater by Fenton's oxidation, ozone and coagulation-flocculation processes, Water Res. 39 (2005) 1147-1153.

[8] G. Ruppert, R. Bauer, G. Heisler, The photo-Fenton reaction-an effective photochemical wastewater treatment process, J. Photoch. Photobio. A 73 (1993) 75-78.

[9] J. T. Spadaro, L. Isabelle, V. Renganathan, Hydroxyl radical mediated degradation

of azo dyes: evidence for benzene generation, Environ. Sci. Technol. 28 (1994) 1389-1393.

[10] S. B. Wang, A comparative study of Fenton and Fenton-like reaction kinetics in decolourisation of wastewater, Dyes Pigments 76 (2008) 714-720.

[11] T. S. Natarajan, K. Natarajan, H. C. Bajaj, R. J. Tayade, Enhanced photocatalytic activity of bismuth-doped TiO_2 nanotubes under direct sunlight irradiation for degradation of Rhodamine B dye, J. Nanopart. Res. 15 (2013) 1-18.

[12] M. Y. Zhu, G. W. Diao, Synthesis of porous Fe_3O_4 nanospheres and its application for the catalytic degradation of xylenol orange, J. Phys. Chem. C 115 (2011) 18923-18934.

[13] H. Seema, K. C. Kemp, V. Chandra, K. S. Kim, Graphene-SnO_2 composites for highly efficient photocatalytic degradation of methylene blue under sunlight, Nanotechnology 23 (2012) 355705.

[14] R. Saravanan, S. Karthikeyan, V. K. Gupta, G. Sekaran, V. Narayanan, A. Stephen, Enhanced photocatalytic activity of ZnO/CuO nanocomposite for the degradation of textile dye on visible light illumination, Mater. Sci. Eng. C 33 (2013) 91-98.

[15] S. Liu, J. Q. Tian, L. Wang, Y. L. Luo, X. P. Sun, One-pot synthesis of CuO nanoflower-decorated reduced graphene oxide and its application to photocatalytic degradation of dyes, Catal. Sci. Technol. 2 (2012) 339-344.

[16] J. Y. Liao, H. Li, X. B. Zhang, D. S. Xiao, N. Qiang, Facile fabrication of Ti supported CuO film composed of bamboo-leaf-like nanosheets and their high catalytic performance in the oxidative degradation of methylene blue with

hydrogen peroxide, Appl. Catal. A 491 (2015) 94-99.

[17] H. Li, J. Y. Liao, Y. C. Du, T. You, W. W. Liao, L. L. Wen, Magnetic-field-induced deposition to fabricate multifunctional nanostructured Co, Ni, and CoNi alloy films as catalysts, ferromagnetic and superhydrophobic materials, Chem. Commun. 49 (2013) 1768-1770.

[18] K. An, G. A. Somorjai, Size and shape control of metal nanoparticles for reaction selectivity in catalysis, ChemCatChem 4 (2012) 1512-1524.

[19] G. M. Whitesides, B. Grzybowski, Self-assembly at all scales, Science 295 (2002) 2418-2421.

[20] R. Srivastava, M. U. A. Prathap, R. Kore, Morphologically controlled synthesis of copper oxides and their catalytic applications in the synthesis of propargylamine and oxidative degradation of methylene blue, Colloid Surface A 392 (2011) 271-282.

[21] M. Q. Yang, J. H. He, Fine tuning of the morphology of copper oxide nanostructures and their application in ambient degradation of methylene blue, J. Colloid Interf. Sci. 355 (2011) 15-22.

[22] N. D. Hoa, N. V. Quy, H. Jung, D. Kim, H. Kim, S. K. Hong, Synthesis of porous CuO nanowires and its application to hydrogen detection, Sensor Actuat. B 146 (2010) 266-272.

[23] X. C. Jiang, T. Herricks, and Y. N. Xia, CuO nanowires can be synthesized by heating copper substrates in air, Nano Lett. 2 (2002) 1333-1338.

[24] Z. J. Zhuang, X. D. Su, H. Y. Yuan, Q. Sun, D. Xiao, M. M. F. Choi, An improved

sensitivity non-enzymatic glucose sensor based on a CuO nanowire modified Cu electrode, Analyst 133 (2008) 126-132.

[25] H. J. Qiu, L. Peng, X. Li, H. T. Xu, Y. Wang, Using corrosion to fabricate various nanoporous metal structures, Corros. Sci. 92 (2015) 16-31.

[26] Z. H. Zhang, Y. Wang, Z. Qi, W. H. Zhang, J. Y. Qin, J. Frenzel, Generalized fabrication of nanoporous metals (Au, Pd, Pt, Ag, and Cu) through chemical dealloying, J. Phys. Chem. C 113 (2009) 12629-12636.

[27] X. Y. Lang, A. Hirata, T. Fujita, M. W. Chen, Nanoporous metal/oxide hybrid electrodes for electrochemical supercapacitors, Nat. Nanotechnol. 6 (2011) 232-236.

[28] R. Li, X. J. Liu, H. Wang, Y. Wu, Z. P. Lu, Bendable nanoporous copper thin films with tunable thickness and pore features, Corros. Sci. 104 (2016) 227-235.

[29] J. S. Yu, Y. Ding, C. X. Xu, A. Inoue, T. Sakurai. M. W. Chen, Nanoporous metals by dealloying multicomponent metallic glasses, Chem. Mater. 20 (2008) 4548-4550.

[30] R. Li, X. J. Liu, H. Wang, Y. Wu, X. M. Chu, Z. P. Lu, Nanoporous silver with tunable pore characteristics and superior surface enhanced Raman scattering, Corros. Sci. 84 (2014) 159-164.

[31] Z. Zhang, Y. Wang, Z. Qi, W. Zhang, J. Qin, J. Frenzel, Generalized fabrication of nanoporous metals (Au, Pd, Pt, Ag, and Cu) through chemical dealloying, J. Phys. Chem. C 113 (2009) 12629-12636.

[32] Z. Qi, C. Zhao, X. Wang, J. Lin, W. Shao, Z. Zhang, X. Bian, Formation and

characterization of monolithic nanoporous copper by chemical dealloying of Al−Cu alloys, J. Phys. Chem. C 113 (2009) 6694-6698.

[33] R. Li, X. Liu, H. Wang, D. Zhou, Y. Wu, Z. Lu, Formation mechanism and characterization of nanoporous silver with tunable porosity and promising capacitive performance by chemical dealloying of glassy precursor, Acta Mater. 105 (2016) 367-377.

[34] X. Luo, R. Li, L. Huang, T. Zhang, Nucleation and growth of nanoporous copper ligaments during electrochemical dealloying of Mg-based metallic glasses, Corros. Sci. 67 (2013) 100-108

[35] A. Gonçalves, L. Campos, A. Ferlauto, R. Lacerda, On the growth and electrical characterization of CuO nanowires by thermal oxidation, J. Appl. Phys. 106 (2009) 034303.

[36] M. Zhong, D. Zeng, Z. Liu, H. Yu, X. Zhong, W. Qiu, Synthesis, growth mechanism and gas-sensing properties of large-scale CuO nanowires, Acta Mater. 58 (2010) 5926-5932.

[37] S. F. Zheng, J. S. Hu, L. S. Zhong, W. G. Song, L. J. Wan, Y. G. Guo, Introducing dual functional CNT networks into CuO nanomicrospheres toward superior electrode materials for lithium-ion batteries, Chem. Mater. 20 (2008) 3617-3622.

[38] J. Fan, Y. H. Guo, J. J. Wang, M. H. Fan, Rapid decolorization of azo dye methyl orange in aqueous solution by nanoscale zerovalent iron particles, J. Hazard. Mater. 166 (2009) 904-910.

[39] Y. Tang, Y. Shao, N. Chen, X. Liu, S. Q. Chen, K. F. Yao, Insight into the high

reactivity of commercial Fe-Si-B amorphous zero-valent iron in degrading azo dye solutions, RSC Adv. 5 (2015) 34032-34039.

[40] M. Neamtu, I. Siminiceanu, A. Yediler, A. Kettrup, Kinetics of decolorization and mineralization of reactive azo dyes in aqueous solution by the UV/H_2O_2 oxidation, Dyes Pigments 53 (2002) 93-99.

[41] L. Carlos, D. Fabbri, A. L. Capparelli, A. B. Prevot, E. Pramauro, F. G. Einschlag, Effect of simulated solar light on the autocatalytic degradation of nitrobenzene using Fe^{3+} and hydrogen peroxide, J. Photochem. Photobiol. A 201 (2009) 32-38.

[42] H. L. Lien, W. X. Zhang, Nanoscale Pd/Fe bimetallic particles: Catalytic effects of palladium on hydrodechlorination, Appl. Catal. B 77 (2007) 110-116.

[43] Q. Wang, S. L. Tian, P. Ning, Degradation mechanism of methylene blue in a heterogeneous Fenton-like reaction catalyzed by ferrocene, Ind. Eng. Chem. Res. 53 (2014) 643-649.

Figure captions

Fig. 1. XRD patterns of the bare $Cu_{60}Zr_{35}Al_5$ precursor ribbon, dealloyed nanoporous Cu and as-prepared CuO nanocomposite, respectively.

Fig. 2. (a) Cross-sectional morphology of the dealloyed nanoporous Cu. The inset is the EDS analysis of the cross section. (b) Surface morphology of the nanoporous Cu. (c) Overall SEM image of the free-standing CuO nanocomposite. The inset shows the cross-sectional image of the nanocomposite. (d) Surface morphology of the as-prepared CuO nanocomposite.

Fig. 3. (a) TEM image of a CuO nanowire. (b) SAED pattern taken from the single nanowire. (c) HRTEM image of the as-prepared CuO nanowire.

Fig. 4. (a) High-resolution XPS spectra of Cu 2p of the CuO nanocomposite sample. (b) N_2 adsorption and desorption isotherm of the CuO nanocomposite. The inset shows the corresponding pore-size distribution.

Fig. 5. (a) The UV absorption spectrum of 0.1 g/L MB solution degraded by CuO nanocomposite in the presence of H_2O_2 for different reaction time at 25 ^oC. The inset is the appearance and color of the MB solution before and after the degradation treatment. (b) The normalized concentration of MB solution at 665 nm as function of reaction time in the presence of different catalysts at room temperature.

Fig. 6. Effect of different variables on the degradation of MB solution by as-prepared CuO nanocomposite: (a) initial H_2O_2 concentration. (b) CuO nanocomposite dosage. (c) initial MB concentration. (d) reaction temperature. The inset is the Arrhenius plot of ln k_T versus $1000/RT$ of MB oxidative degradation by CuO nanocomposite.

Fig. 7. (a) Degradation ration of 0.1 g/L MB solution by 2 g/L CuO nanocomposite for 70 min at different cycles (room temperature). (b) Surface morphology of the nanostructured CuO after 5 catalytic cycles. The inset is the EDX analysis of the surface of the treated sample.

Fig. 1 by Li et al.

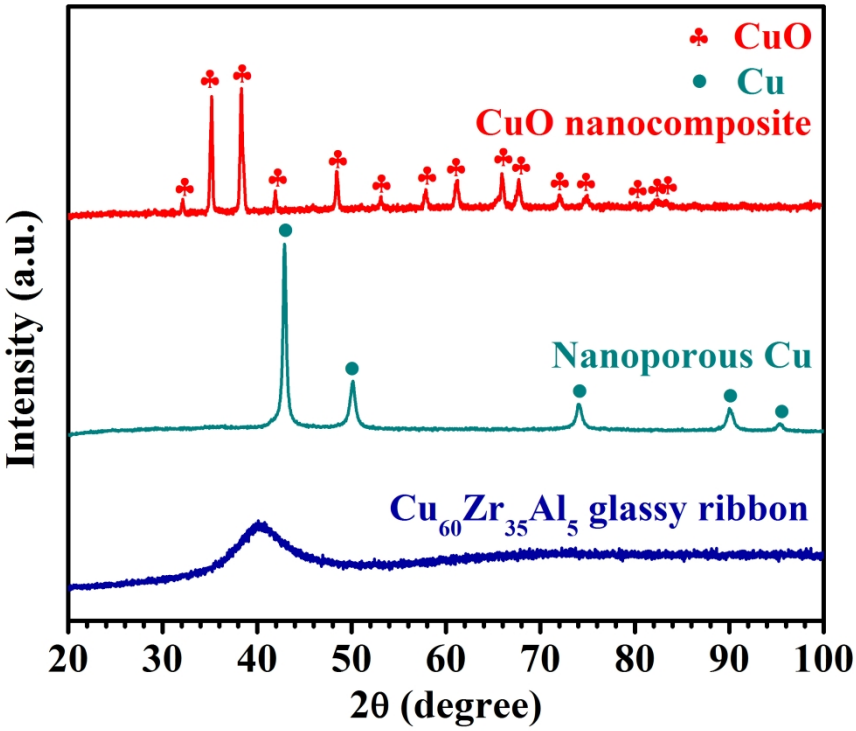

Fig. 2 by Li et al.

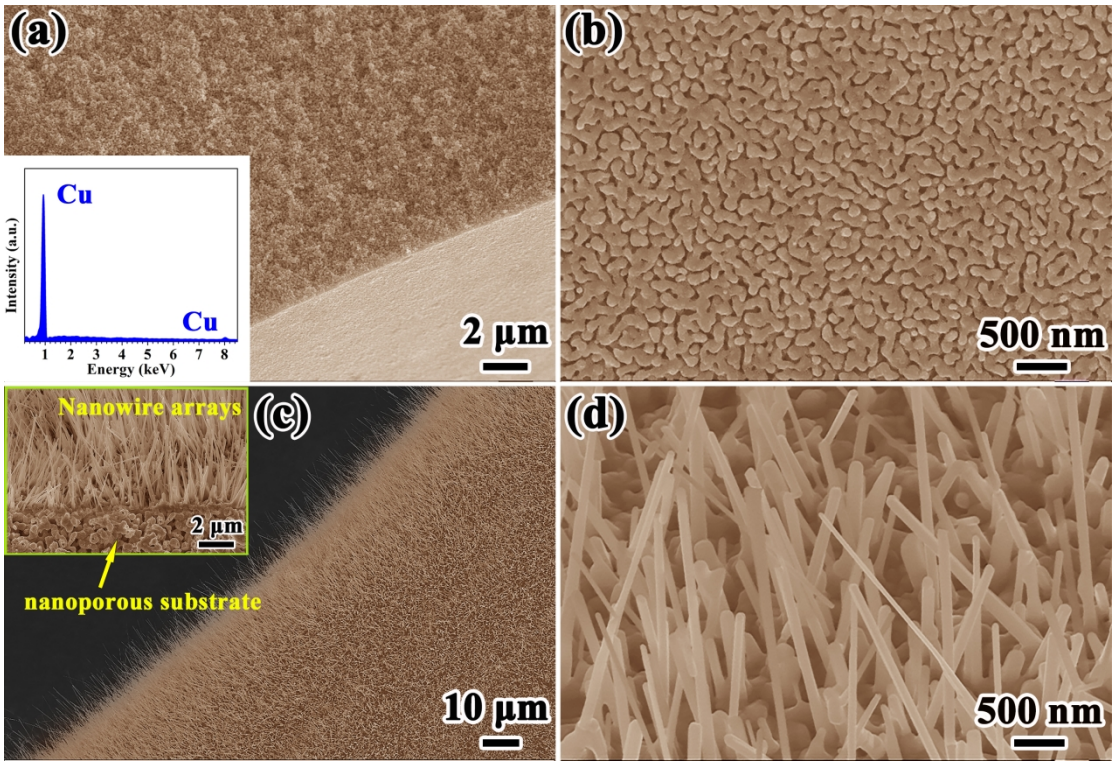

Fig. 3 by Li et al.

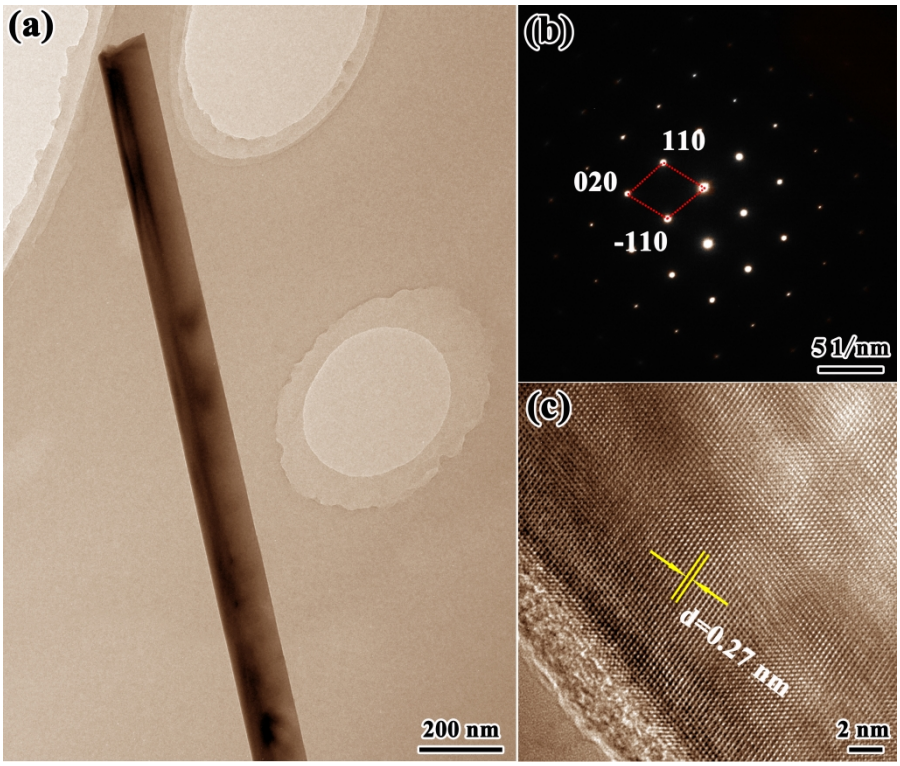

Fig. 4 by Li et al.

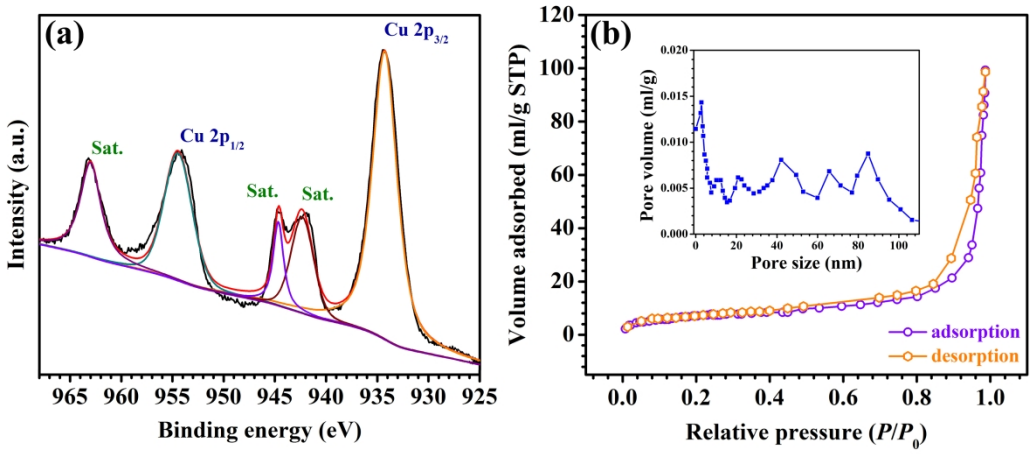

Fig. 5 by Li et al.

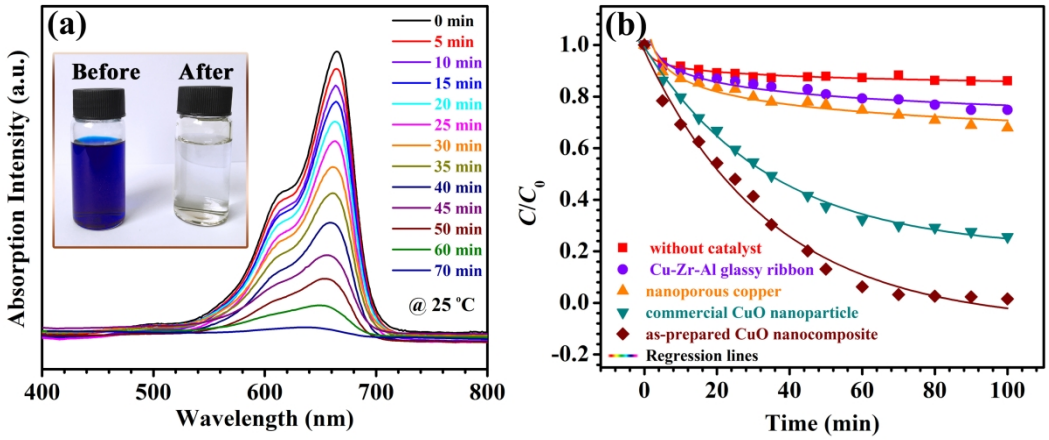

Fig. 6 by Li et al.

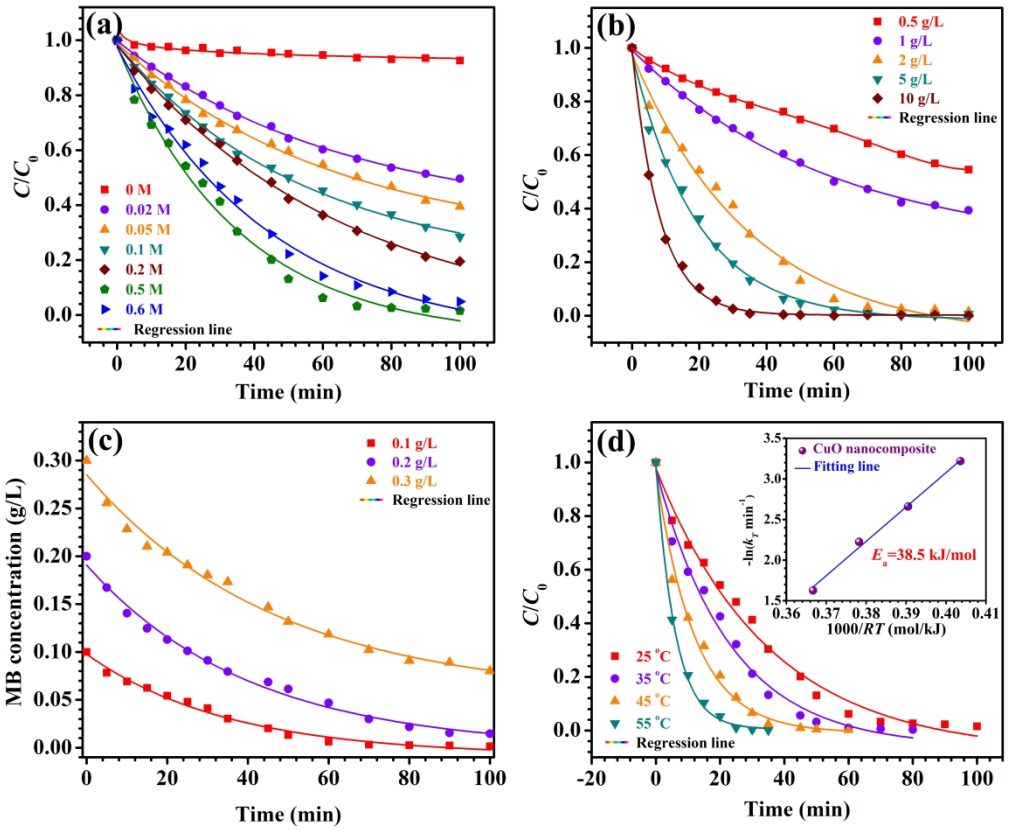

Fig. 7 by Li et al.